SEPARATA

Revista Geológica de Chile 35 (1): 105-121. January, 2008

Revista Geológica de Chile

Long-term denudation rates from the Central Andes (Chile) estimated from a Digital Elevation Model using the Black Top Hat function and Inverse Distance Weighting: implications for the Neogene climate of the Atacama Desert

Rodrigo Riquelme[1], José Darrozes[2], Eric Maire[2], Gérard Hérail[2,3], J. C. Soula[2]

[1] *Departamento de Ciencias Geológicas, Facultad de Ingeniería y Ciencias Geológicas, Universidad Católica del Norte, Avda. Angamos 0610, Antofagasta, Chile.*
rriquelme@ucn.cl

[2] *Laboratoire des Mécanismes et Transferts en Géologie, Université de Toulouse-Institut de Recherche pour le Développement (IRD)-Centre National de la Recherche Scientifique (CNRS), 14 avenue Edouard Belin, 31400, Toulouse, France.*
darrozes@lmtg.obs-mip.fr; maire@lmtg.obs-mip.fr; soula@lmtg.obs-mip.fr; gerard.herail@ird.fr

[3] *Departamento de Geología, Universidad de Chile, Plaza Ercilla 803, Santiago, Chile.*

ISSN 0716-0208
Editada por el Servicio Nacional de Geología y Minería
con la colaboración científica de la Sociedad Geológica de Chile
Avda. Santa María 0104, Casilla 10465, Santiago, Chile.
revgeologica@sernageomin.cl; http://www.scielo.cl/rgch.htm; http://www.sernageomin.cl

Revista Geológica de Chile 35 (1): 105-121. January, 2008

Revista Geológica de Chile

www.scielo.cl/rgch.htm

Long-term denudation rates from the Central Andes (Chile) estimated from a Digital Elevation Model using the Black Top Hat function and Inverse Distance Weighting: implications for the Neogene climate of the Atacama Desert

Rodrigo Riquelme[1], José Darrozes[2], Eric Maire[2], Gérard Hérail[2,3], J. C. Soula[2]

[1] *Departamento de Ciencias Geológicas, Facultad de Ingeniería y Ciencias Geológicas, Universidad Católica del Norte, Avda. Angamos 0610, Antofagasta, Chile.*
rriquelme@ucn.cl

[2] *Laboratoire des Mécanismes et Transferts en Géologie, Université de Toulouse-Institut de Recherche pour le Développement (IRD)-Centre National de la Recherche Scientifique (CNRS), 14 avenue Edouard Belin, 31400, Toulouse, France.*
darrozes@lmtg.obs-mip.fr; maire@lmtg.obs-mip.fr; soula@lmtg.obs-mip.fr; gerard.herail@ird.fr

[3] *Departamento de Geología, Universidad de Chile, Plaza Ercilla 803, Santiago, Chile.*

ABSTRACT. A methodology for determining long-term denudation rates from morphologic markers in a Digital Elevation Model (DEM) is checked by a comparative study of two drainage basins in the Precordillera of the Central Andes. In both cases the initial configuration of an incised pediment surface has been restored by using two different methods: the Black Top Hat (BTH) function and the Inverse Distance Weighting (IDW) interpolation. Where vertical incision and hillslope erosion are recorded, the IDW appears to be the most adequate to reconstitute the pediment surfaces. Conversely, where only vertical incision is observed, the BTH describes more precisely the former pediment surfaces and it is easier to solve. By subtracting the DEM from the reconstructed marker we calculated an eroded volume, and estimated its uncertainty by considering Root Mean Square Error (RMSE) and DEM grid error. For the last ~10 Myr we obtained long-term denudation rates of 7.33±1.6 m/Myr in the San Andrés drainage basin and 13.59±1.9 m/Myr in the El Salado drainage basin. These estimations are largely in agreement with other reported estimates of long-term denudation rates in the Atacama Desert. Comparison with long-term denudation rates reported in a wide range of climatic regimes suggests that our estimates cannot be explained by the current rainfall in the Precordillera. However they could be explained by a rainfall similar to that reported 40 km to the east in the Puna. This suggests that during the time span concerned the geomorphologic evolution of the study area, this evolution is dominated by an orographically controlled rainfall pattern. The preserved pediment surface and the small long term denudation rates determined in this study also indicate that the Precordillera was never reached by humid tropical air masses and precipitation as currently observed in the Altiplano during the summer months.

Keywords: Quantitative geomorphology, DEM, Andes, Long-term denudation, Black Top Hat.

RESUMEN. Tasas de denudación de largo tiempo en los Andes Centrales, Chile, estimadas a partir de un modelo digital de elevación usando la función 'Top Hat' por cierre y la interpolación ponderada por el inverso de la distancia: implicancias del clima Neógeno del Desierto de Atacama. Una metodología para determinar tasas de denudación de largo tiempo a partir de marcadores geomorfológicos obtenidos desde un Modelo Digital de Elevación (MDE), ha sido comprobada considerando un estudio comparativo de dos cuencas vertientes de la precordillera de los Andes Centrales. Para ambas cuencas, la configuración inicial de una superficie de pedimentación afectada por incisión, ha sido reconstruida usando dos métodos diferentes: la función 'Top Hat' por Cierre (THC) y la Interpolación Ponderada por el Inverso de la Distancia (IPID). Cuando se observa tanto incisión vertical como erosión de laderas, la IPID es más apropiada para reconstruir las superficies de pedimentación. Por el contrario, donde solo se observa incisión vertical, la THC describe con mayor precisión las superficies de pedimentación, y es de más fácil implementación. En este trabajo, se calculó un volumen erosionado por medio de la sustracción del MDE del marcador geomorfológico reconstruido, y se estimó su incertitud al considerar un Error Cuadrático Medio y un MDE representando una grilla de errores. Para los últimos 10 Myr se obtuvo tasas de denudación de largo tiempo de 7,33±1,6 m/Myr en la cuenca vertiente de San Andrés y de 13,59±1,9 m/Myr en la cuenca vertiente de El Salado. Estas estimaciones son similares a otras estimaciones de tasas de denudación de largo tiempo publicadas para el Desierto de Atacama. La comparación con valores de tasas de denudación de largo tiempo reportadas para un amplio rango de regímenes climáticos sugiere que estas estimaciones no pueden ser explicadas por las actuales tasas de precipitación de la Precordillera. Sin embargo, podrían ser explicadas por tasas de precipitación similares a aquellas actualmente imperantes 40 km al este, en la Puna. Esto sugiere que durante el lapso de tiempo concerniente a la evolución geomorfológica del área de estudio, esta evolución es dominada por el control orográfico de las precipitaciones. La preservación de superficies de pedimentación y los bajos valores de las tasas de denudación de largo tiempo determinadas en este estudio indican, por otra parte, que la Precordillera no fue afectada por precipitaciones y masas de aire húmedas tropicales como las que actualmente se observan en el Altiplano durante los meses de verano.

Palabras claves: Geomorfología cuantitativa, MDE, Andes, Denudación de largo tiempo, 'Top Hat' por Cierre.

1. Introduction

Denudation rates result from the interaction between the relative effects of erosion, tectonics and climate on landscape evolution. Knowledge of long-term denudation rates (100 ky to 10 Ma) and understanding the factors that control them are important for a number of reasons. They allow the description of the nature and rates of geomorphic processes that control landscape evolution. Realistic estimations of long-term denudation rates must be considered when interaction between tectonic and subaerial processes is explored, for instance, by using quantitative landscape evolution models (Ahnert, 1970; Beaumont *et al*., 1996; Howard, 1997; Whipple and Tucker, 1999; Coultard, 2001). Comparison of long-term denudation and uplift rates can also be used to establish the degree of equilibrium reached by the landscape (*e.g.*, Meigs *et al.*, 1999; Carretier and Lucazeau, 2005). Long-term denudation rates are a vital component of mass balances studies aimed at understanding the factors that perturb the global carbon budget and consequently influence global climate (Raymo *et al*., 1988; Raymo and Ruddiman, 1992). A knowledge of the long-term denudation rate and its comparison with the current sediment and solute yields of rivers, would allow discussion, for instance, of the relative impact of paraglacial sediment reworking (*i.e*., sediment reworking occurred after the Last Maximum Glacial Advance) or anthropogenic effects on the sediment delivery by rivers draining the northern and central Chilean Andes.

In order to quantify long-term denudation rates different methods have been applied, including: thermochronology (*e.g*., Maksaev and Zentilli, 1999), cosmogenic nuclide methods (*i.e*., Riebe *et al*., 2000), and determination of sediment and solute yields in a drainage basin (*i.e*., Probst and Suchet, 1992; Guyot, 1993). These methods require arduous and expensive analytical techniques, and they present discrepancies when comparing different spatial and temporal scales. Alternatively, when ages of relatively well preserved morphologic surfaces (*e.g.*, pedimentation surface) are available, denudation rates can be estimated from reconstruction of the surfaces in a Digital Elevation Model (DEM). In this way, the Black Top Hat (BTH) function was applied in order to estimate the incised volume in a river valley (Rodríguez *et al*., 2002).

The purpose of this paper is to discuss the benefit of the application of the BTH function to

the estimation of the long-term denudation rates for rejuvenated topography (Fig. 1b-c). We use a DEM generated by interpolation of digitized contour lines of 1:50,000 topographic maps, resulting in a 40 m horizontal DEM resolution and a vertical error range of ±10 m. The BTH method is of limited use in some cases, notably where a smooth morphology representing a relict topography affected by current hillsope erosion is present (Fig. 1b). In this case, an alternative methodology for reconstructing morphologic surfaces, and consequently, estimating long-term denudation rates is proposed. We discuss the results obtained from the application of the BTH and the alternative method on two drainage basins located on the western slope of the Central Andes (Fig. 1a). We focus on the determination and propagation of the uncertainties associated with both the base-DEM used, and the morphologic reconstruction, in order to evaluate the uncertainties in the denudation rate.

Furthermore, we propose an objective and effective criterion to recognize if the BTH function should or should not be applied to the considered landscape. Finally, our denudation rates obtained will be compared to those estimated by other methods.

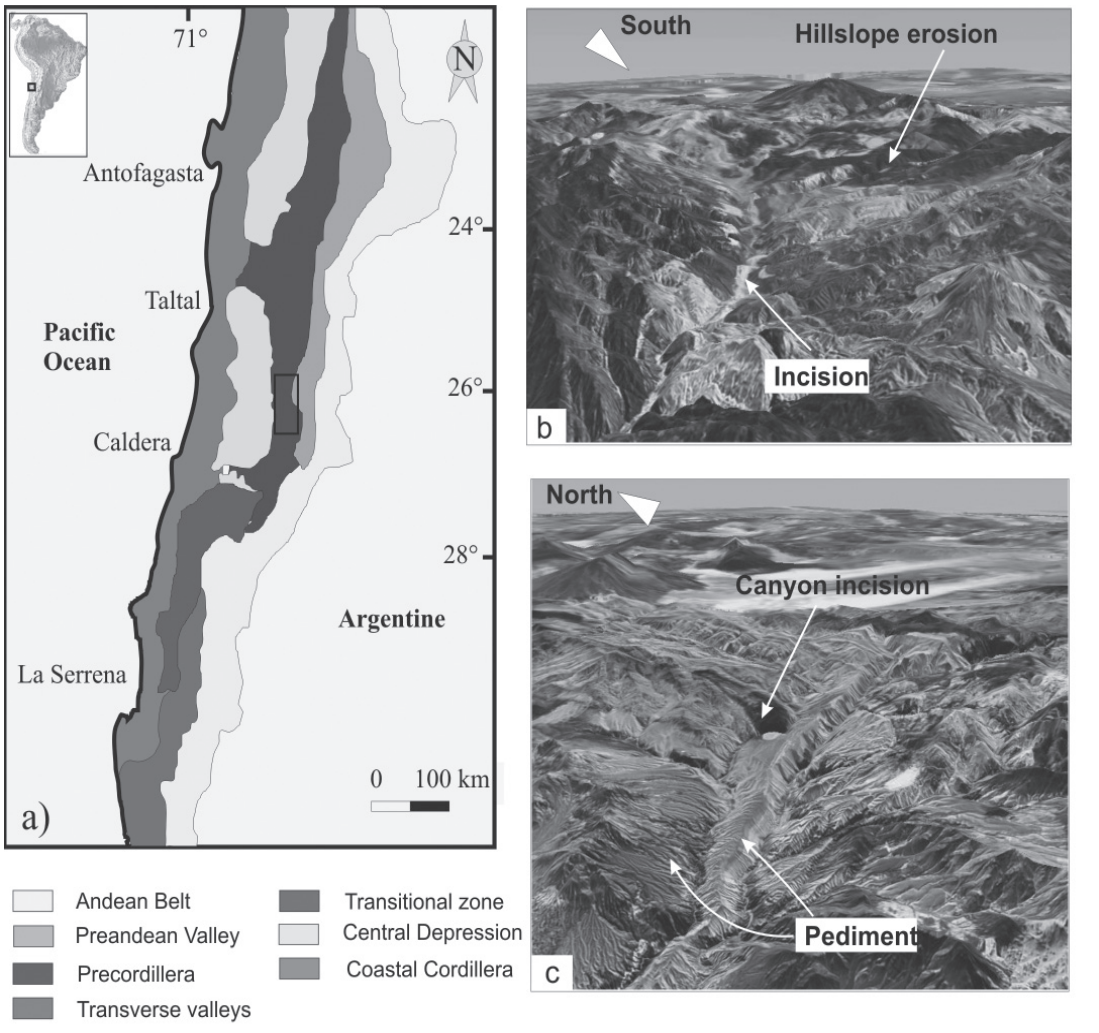

FIG. 1. **a.** Location and morpho-structural sketch map of the study area; Digital Elevation Model (DEM) and superimposed Landsat 1-4-7 channels are shown; **b.** NE 3D view of the San Andrés Basin (elevation range: 2,500-4,000 m, area ≈1300 km^2); **c.** ENE 3D view of El Salado Basin (elevation range: 1,000-5,800 m, area ≈1300 km^2). Vertical exaggeration for b) and c): x^3.

2. The test areas: the San Andrés and El Salado basins in the northern Chilean Andes

The studied basins are located in the Precordillera of northern Chile in the southern Atacama Desert, between 26º and 28ºS. (Fig. 1). In this region an arid climatic regime has been dominant since the Middle Miocene (Alpers and Brimhall, 1988; Sillitoe and McKee, 1996; Nishiizumi *et al*., 2005) and the present hyperarid climate was established in the Late Pliocene (Hartley and Chong, 2002). These climate conditions are responsible for Neogene geomorphologic evolution of the study area and the formation of an extensive pedimentation surface (Atacama Pediplain of Sillitoe *et al*., 1968). This pedimentation surface occupies most of the topography of the El Salado and San Andrés Basins. K-Ar ages of 11.5±0.5 Ma, 9.5±0.5 Ma, 9.0±0.3 Ma (Sillitoe *et al*., 1967), 10.2±0.9 Ma (Cornejo *et al*., 1993)[1] and a Ar/Ar age of 9.19±0.61 Ma (Riquelme *et al*., 2007) have been recorded in an ignimbrite deposit that covers the pedimentation surface in the Precordillera, between 26°-27°S. The ignimbrite level marks the end of the alluvial fan landscape infilling related to pedimentation processes and the beginning of the strong vertical incision (up to 800 m) that generated the current drainage basin systems (Mortimer, 1973; Riquelme *et al*., 2007). The interpreted evolution is corroborated by the exposure age of cobbles collected on alluvial fan surfaces that compose the Atacama Pediplain in the Precordillera: based on combined measurements of ^{10}Be, ^{26}Al, and ^{21}Ne concentrations, Nishiizumi *et al*. (2005) proposed, an age of 9 Ma for the beginning of the incision of the Atacama Pediplain.

The vertical canyon incision is probably active today, but hillslope erosion related to headward propagation of the drainage is also observed. We have studied two drainage basins of the Atacama Desert which contain both the pedimentation surface and the ignimbrite level, the latter providing a good time constraint on the start of incision: (1) the San Andrés Basin, where canyon incision as well as hillslope erosion can be observed (Fig. 1b) and (2) the El Salado Basin, where only canyon incision took place (Fig. 1c).

The main structural system exposed in this region corresponds to the Domeyko Fault System (DFS). The last major deformational events accommodated by the DFS correspond to the Eocene-Early Oligocene 'Incaic' tectonic phase, and are responsible for most of the important structures in the region (Cornejo and Mpodozis[2], 1996; Tomlinson *et al*., 1994; Randall *et al*., 2001). The orientation and style of these structures control the distribution of the lithologic units and the shape of the El Salado and San Andrés Basins (Fig. 2). In the El Salado Basin, the DFS comprises the subvertical Sierra Castillo Fault (SCF) which juxtaposes Paleozoic batholithic rocks on the east against Jurassic and Cretaceous volcanic sequences on the west. To the east, the east-vergent Potrerillos fold and thrust belt deforms primarily a Mesozoic platform carbonate and clastic sequence and is oriented parallel to the elongation of the El Salado Basin (Cornejo *et al*., 1993[1]; Tomlinson *et al*., 1994) (Fig. 2). In the San Andrés Basin, the DFS exposes the moderately to steeply west dipping Agua Amarga Fault (AAF) places the Jurassic and Cretaceous volcanic sequences on the west over Paleocene-Eocene volcanic units on the east. This fault forms the western water divide of the San Andrés Basin. The north-eastern water divide exposes the Mesozoic carbonate and clastic sequence and coincides with a set of northwest-trending subvertical faults that belong to the DFS (Tomlinson *et al*., 1994; Randall *et al*., 2001).

3. Volume Estimation Methodologies

3.1. Top Hat Formalism and its limits

The Top Hat Transform function is a mathematical morphology function which allows peak and valley extraction in a 1D signal and 2D image. Efficiency of the 'Top Hat' Transform was demonstrated by Meyer (1979) for Cytology applications. In geomorphology, this function was applied to a high-precision DEM as a relevant tool for estimating incision and the amount of material removed by recent fluvial erosion in a Pyrenean watershed (Rodríguez *et al*., 2002). The mathematical formulation is based on a set

[1] Cornejo, P.; Mpodozis, C.; Ramírez, C.F.; Tomlinson, A.J. 1993. Estudio Geológico de la Región de Potrerillos y El Salvador (26°-27°S). Servicio Nacional de Geología y Minería-CODELCO, Informe Registrado IR-93-01, 258 p., 12 cuadrángulos escala 1:50.000. Santiago, Chile.

[2] Cornejo, P.; Mpodozis, C. 1996. Geología de la Región de Sierra Exploradora (Cordillera de Domeyko, 25°-26°S). Servicio Nacional de Geología y Minería-CODELCO, Informe Registrado IR-96-09, 330 p. Santiago, Chile.

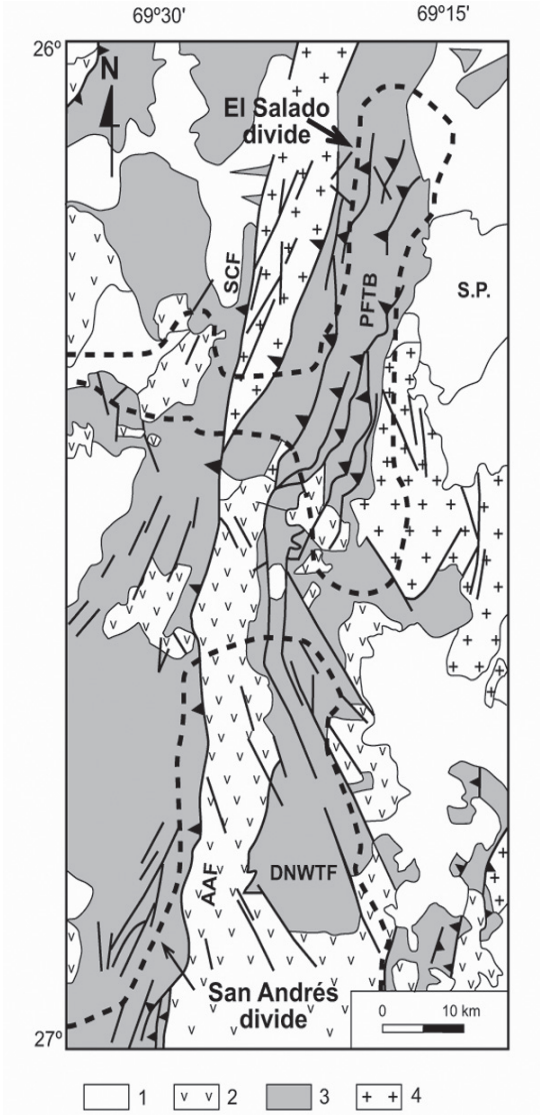

FIG. 2. Simplified geological map of the study area showing: **1.** Oligocene-Quaternary gravel deposits; **2.** Upper Cretaceous-Lower Eocene volcanic rocks; **3.** Triassic-Cretaceous volcanic and sedimentary rocks; **4.** Paleozoic granitoids and volcanic rocks. SCF Sierra Castillo Fault, PFTB Potrerillos Fold and Thrust Belt, AAF Agua Amarga Fault, DNWTF Domain N-W trending fault. **S.P.:** Salar de Pedernales. Modified from Tomlinson *et al.* (1994).

of mathematical morphology concepts presented in appendix A. This formulation is provided by a number of specialized software for landscape image processing.

A DEM is a grey-tone image where, normally, clear zones represent landscape regions of relatively higher elevations, whereas dark zones represent regions of relatively lower elevation. A DEM can be viewed as a function where f(x) represents the elevation (generally grey levels) in a pixel located at the coordinate x. Considering the elementary grey level mathematical morphology operations: let λ a structuring element centred on x and y the considered point (pixel). The initial DEM (Fig. 3a) is transformed by dilation and erosion using the equations A8 and A9, respectively (see appendix A). Dilation of the DEM is presented for lengths of λ equal to 2 pixel (Fig. 3b) and L pixels (Fig. 3c). The dilated DEM of figure 3c is then eroded for a length of λ equal to L pixels, resulting in the image of figure 3d and 2e.

Dilation of the image f(x) to obtain the image of figure 3c, followed by erosion of the later resulting in the image of figure 3e, constitutes the closing transformation of the initial DEM for a structuring element λ of length equal to L pixels (eq. A5 of appendix A). The closing transformation is commonly used to join clear zones (lightest grey levels) while the opening transformation (eq. A6 of appendix A) is used to separate them. The closing and opening transformations are the basis of the Top Hat Transform formalism. The Black Top Hat (BTH) transformation uses the closing procedure and is defined as follow:

$$BTH = \{x: C_{\lambda}(x) - f(x) \geq t\} \qquad (1)$$

It allows the extraction of valleys in a grey-tone level (elevation) image by subtraction of the image of closed valleys $C_{\lambda}(X)$ and the initial image f(x) (Fig. 3f). The transformation considers a size condition equal to the size L for a given structuring element λ (Meyer, 1979) and a threshold t (Fig. 3g). The threshold value t allows the extraction of valleys without the topographic noise, which corresponds to the darkest grey-levels (Fig. 3h). Hence, only the information for the deepest valleys is kept (Rodríguez *et al*., 2002).

The application of the BTH function is based on the selection of the length L, which corresponds to the width of the valley to be extracted. In our case, the width corresponds to the greatest separation between pedimentation surfaces throughout the valleys for the entire basin. Therefore, a good reconstruction of the pedimentation surfaces can be achieved only if the hillslope gradients are high and if the inflection point between the preserved

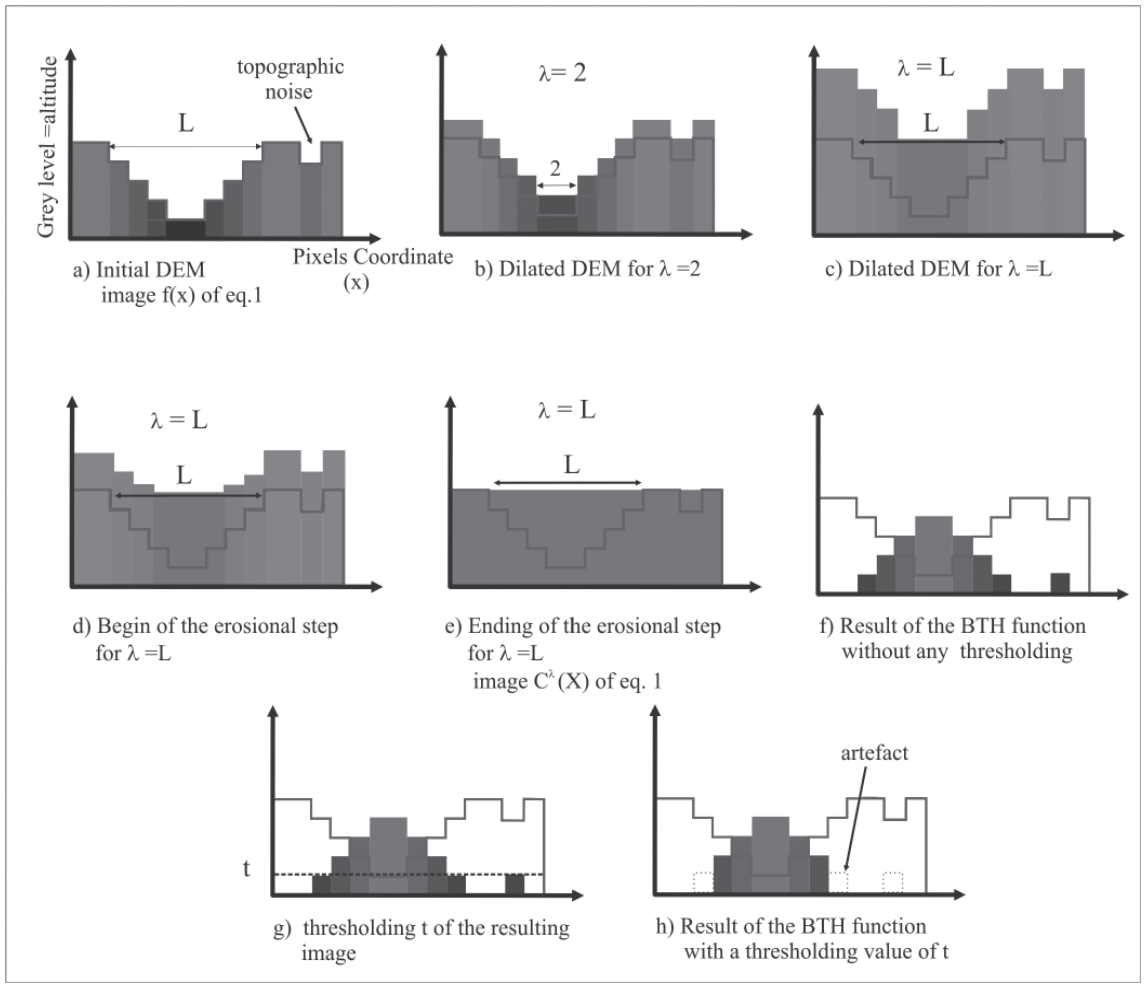

FIG. 3. Diagram showing the application of the BTH function and the estimation of an eroded volume from a DEM: **a.** initial DEM with a random noise (artefact of DEM); **b.** dilatation of the DEM for a length of λ equal to 2 ('λ=2'), the smallest valleys are closed; **c.** dilation of the DEM for a length of λ equal to L, the main valleys are now closed but the elevation of the picks around the valleys increased. To return to the initial elevation of the peaks, the image should be eroded; **d.** the beginning of the erosive process effectively decreases peak elevations without modifying the valley zones; **e.** resulting C^{λ} (x) image, the valleys are closed without modifying the rest of the image; **f.** result of the BTH function: C^{λ} (x)-f(x), gives the eroded volume of the valleys plus that of the noise zones; **g.** the threshold value t makes it possible to remove the noise zones; **h.** Result after thresholding, notice the disappearance of the noise zones on the edges of the eroded volume.

surface and the hillslope is properly defined. This would be the case in a rejuvenated landscape with canyon formation. However, if the surface has low hillslope gradients, such as a preserved pedimentation surface, the determination of the length L is poorly defined due to the difficulty of identifying the inflection point.

It is important to note that hillslope erosion in the upper part of the basin can result in a larger separation of the pedimentation surfaces than those in the lower basin. Thus, considering the length of the structuring element as the separation of the remnant pedimentation surfaces in the lower basin, the altitude of the reconstructed surface, and consequently the eroded volume, will be underestimated where hillslope erosion is present (L=3040 m, Fig. 4 volume a_1). Selecting as a length L the maximum separation between surfaces where erosion is present, then the altitude of the reconstructed surface and consequently the eroded

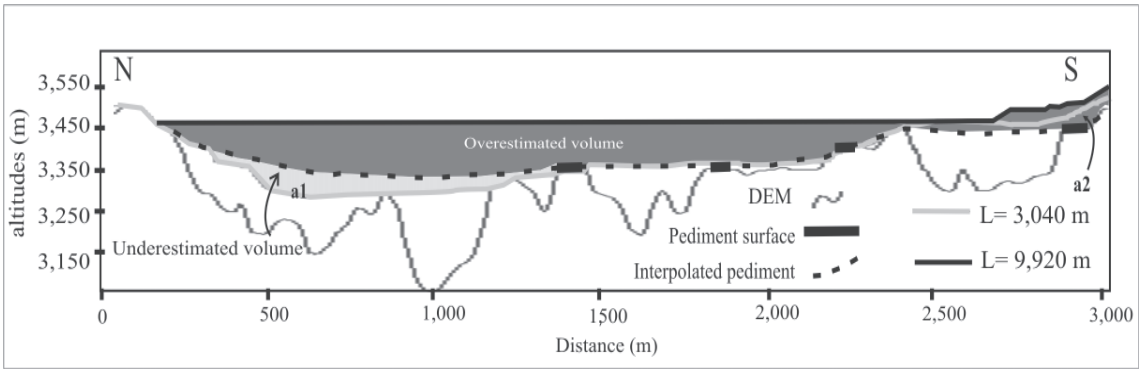

FIG. 4. Profile showing the DEM and the Top Hat reconstruction for the minimum and maximum L that can be selected for the San Andrés basin.

volume, will be locally overestimated (L=9,920 m, Fig. 4 volume a_2). Since the BTH method, in this case, does not lead to a good reconstruction of the pedimentation surface where hillslope erosion is important, an alternative methodology for reconstructing geomorphologic surfaces that better fits this scenario is presented below.

3.2. Reconstruction of Geomorphologic Surface by Inverse Distance Weighting (IDW)

The reconstruction of the pedimentation surfaces is divided into three steps:

a) The first step is selection of points corresponding to the definition of a pedimentation surface (Viers, 1967). This comprises points that **(i)** have a local slope lower than 10°, in fact more generally 0-3° in the lower areas and up to 10° close to the mountains; **(ii)** belong to the mean area±RMS (root mean square) portion in the area *versus* altitudes histogram (Fig. 5a) and correspond to the constant level of the hypsometric curve (Fig. 5b) and **(iii)** do not belong to the present valley bottoms. Using these criteria it is possible to identify the set of points that comprise remnant pedimentation surfaces (Fig. 6b).

b) The second step is the interpolation of the points by the IDW method (Shepard, 1968; Fisher *et al*., 1987). To reconstruct the pedimentation surface, we have selected an Inverse Distance Weighting method. This is a simple algorithm that is designed to avoid the effects of interpolation that could distort the slope of the planated surface determined from the randomly selected points. Alternatively, its mathematical expression (eq. 2) could be considered the approximation of a planated surface (Fig. 7). The interpolation equation is as follows:

$$Z(x,y) = \frac{\sum_{i=1}^{k} \frac{Z_i}{d_i^2} \times C_i}{\sum_{i=1}^{k} \frac{1}{d_i^2} \times C_i} \qquad (2)$$

Where each *Z(x,y)* interpolated grid point is evaluated by considering the k-nearest neighbour point with grey-tone level Z_i and distance d_i from the current grid point being interpolated. C_i is the confidence level that, considering the randomly selected point distribution, has been determined as follows: 100% confidence for the 8 neighbouring points, and 0% confidence for the rest.

c) The last step is the calculation of the eroded volume. The estimation of the eroded volume that allows us to calculate the long-term denudation rate is determined by subtracting the DEM from the reconstructed surface (Fig. 6c). In addition, we have also estimated the uncertainty in the eroded volume associated with both, the uncertainty inherent to the DEM (vertical error range of±10 m), and that of the surface reconstruction. An error grid was then generated for the reconstructed surface that allows us to associate with each pixel grey-level a corresponding grey-level error value (Fig. 6d). The final uncertainty in the volume estimation considers error in elevation associated with each pixel in the DEM (±10 m) and in the reconstructed surface.

In order to generate the error grid we calculated the difference between control points and the corresponding grey-level in the reconstructed

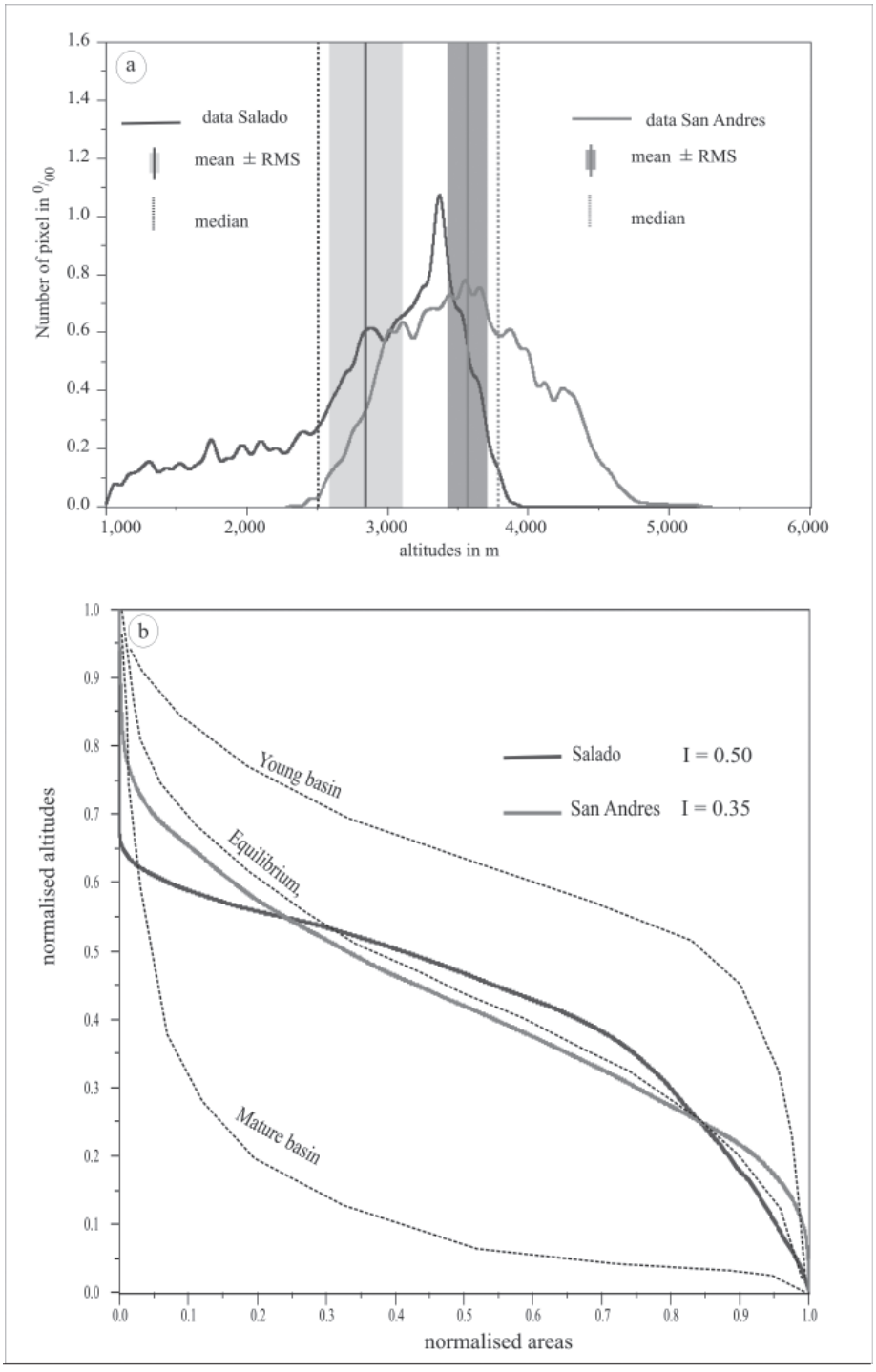

FIG. 5. Hypsometric curves for the San Andrés and El Salado basins: **a.** histogram of altitudes repartition in $^{0}/_{00}$ of pixels and associated statistical parameters; **b.** The normalised hypsometric curves (graph that shows the proportion of land area that exists at various elevations by plotting normalised area against normalised altitudes) and its hypsometric values. Note: I=hypsometric integral value=area under the considered curve. In dashed lines the theoretical curve for a mature basin, a young basin and the equilibrium curve (Strahler, 1952); note that the curves are close to equilibrium, with the overall El Salado curve on top and that of the San Andrés below the equilibrium.

surface. These differences are then interpolated to the entire basin by using a polynomial interpolation function. The control points correspond to a 5%-random sampling as explained in the following sectiom.

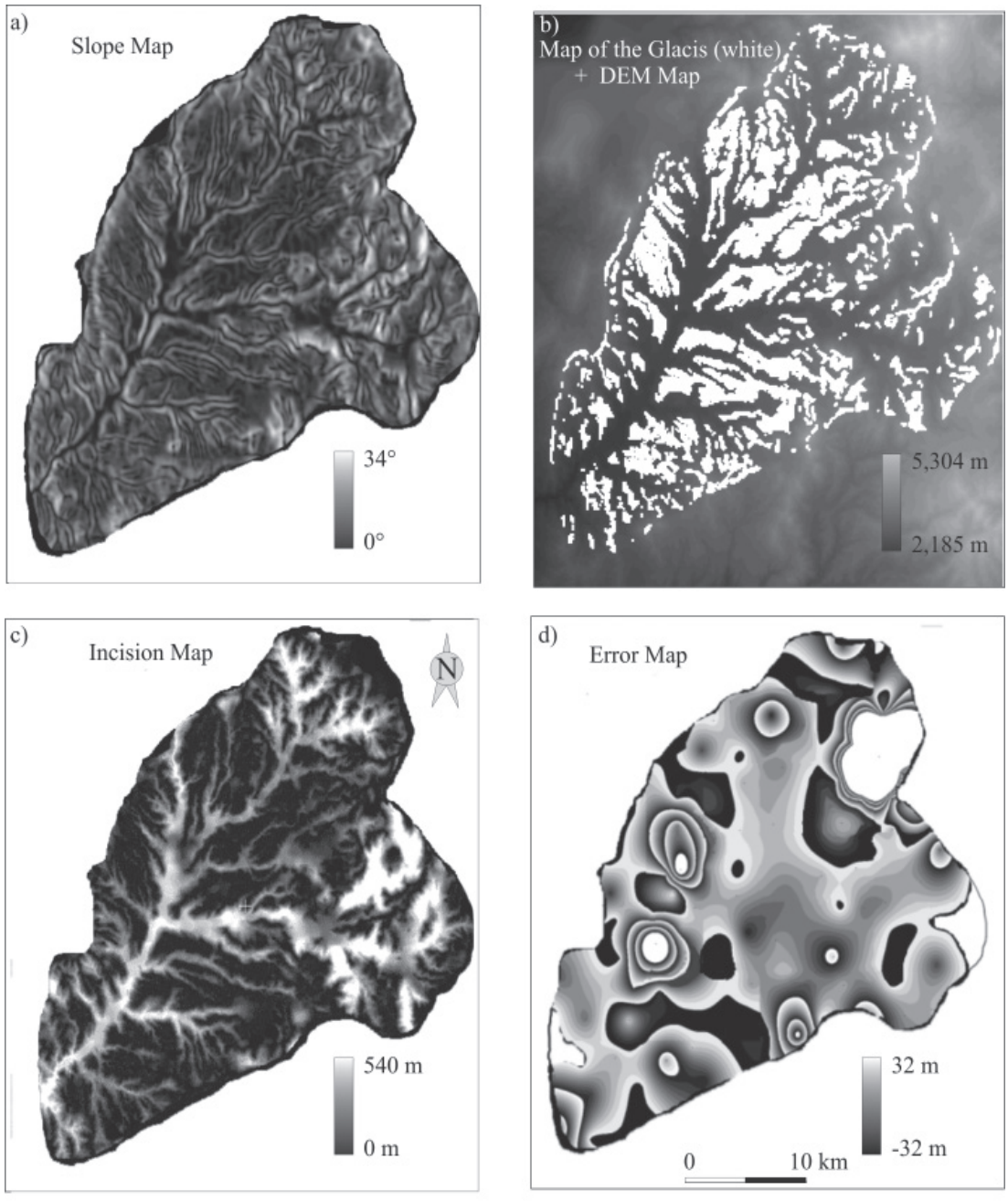

FIG. 6. Schematic stages of the calculation of the incision rate and the associated error in map; **a.** Maximum local slope grid of the San Andrés basin determined from a 5x5 window; **b.** DEM showing, in white, the areas pertaining to the pediment surface identified by the method detailed in the text; **c.** Incision grid (white areas) determined by subtraction of the DEM from the interpolated pediment surface; **d.** Error grid for the interpolated pediment surface. The greater errors are registered in areas of greater slope *i.e.*, the zones where the pediment extension is very restricted.

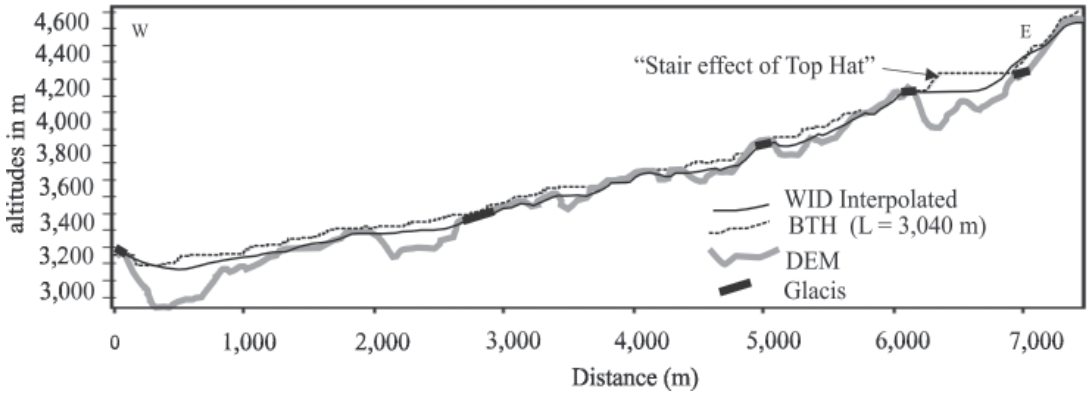

FIG. 7. Profile showing a comparison between the WID reconstruction and the best BTH reconstruction. Notice that BTH reconstruction generates a 'stair effect in the hillslope'.

3.3. Comparison with the BTH

In order to compare the interpolated pedimentation surface with that obtained by the BTH function we used the concept of Root Mean Square Error (RMSE), it is expressed as:

$$RMSE = \frac{\sqrt{\sum_{i=1}^{n}(Z(x,y) - Z_i)^2}}{n} \qquad (3)$$

Where $Z(x,y)$ is an elevation point, *i.e.*, the elevation point of the reconstructed pedimentation surface corresponding to Z_i: the 'true' known or measured test points and n is the number of sampled points. In order to obtain a set of statistically representative test points we have made a 5% random sampling in the remnant pedimentation surfaces for the DEM and both the IDW interpolated and the BTH calculated surfaces. We use a random sampling of 5% because it makes it possible to make a statistically reliable measurement of RMSE (more than 30 samples), and this sample density is also sufficiently precise to represent the correct geometry of the pedimentation surface.

4. Results

4.1. Determination of the present pedimentation surfaces

For San Andrés Basin. The area *versus* altitude histogram of the San Andrés Basin shows a single slightly low-altitude asymmetrical mode (Fig. 5a). The hypsometric integral value I -*i.e.*, the area under the hypsometric curve- is relatively low (Fig. 5b, I=0.35) which represents a rather smoothed landscape surface (Strahler, 1952). By thresholding the altitudes of the DEM, it is possible to select the range of altitudes located between mean area ±Root Mean Square (RMS, Fig. 5a). These correspond essentially to remnant pedimentation surfaces but also include zones where hillslope erosion is present which is consistent with a relatively smoothed landscape surface. The other condition to define the pedimentation surface is a local slope less than 10°. From the DEM-extracted local slope image (Fig. 6a) it is possible to select only points where the slope angle is <10°. From this range of slope values and the range of threshold values we can obtain the points that constitute the remnant pedimentation surfaces (Fig. 6b).

For El Salado Basin. The area *versus* altitude histogram of El Salado is marked by an asymmetrical shape with a predominance of high altitudes (Fig. 5a). The hypsometric integral value is relatively high (Fig. 5b, I=0.50) and can be interpreted as the result of a rejuvenated landscape surface (Strahler, 1954). In the El Salado Basin an older landscape surface (the pedimentation surface) is affected by strong vertical incision (the El Salado canyon). By thresholding the slope and the altitude of the DEM it is possible to observe that the low altitudes mainly correspond to the bottom of canyon and the high altitudes correspond to residual low sloping remnants of the pedimentation surface.

4.2. Comparison between the BTH and IDW methods

We can demonstrate the efficiency of these methods and their limits by the analysis of the Root Mean Square Error (RMSE) obtained by both methods. This analysis combined with the morphology of the basin will allow determination of of the method best adapted to a given morphology.

For the San Andrés Basin the minor RMSE (≈22 m) for the BTH application is obtained when an L=3040 is used (Table 1), whereas a RMSE ≈5 m was obtained for the IDW surface. From the morphological point of view the San Andrés Basin is characterized by a smoothed morphology corresponding to a mature watershed (Strahler, 1952). The morphology of the catchment results from vertical incision of remnant pedimentation surface affected by important hillslope erosion. This type of catchment is easily identifiable either by field analysis or by the hypsometric integral which has a relatively low value (Fig. 5b, I=0.35).

For the El Salado Basin, the RMSE results are inverted (see Table 1); in this case the RMSE for the IDW surface (≈20 m) is twice that obtained by the BTH method (≈9 m). From the geomorphological viewpoint the catchment corresponds to a pedimentation surface affected only by strong vertical incision, *i.e*., reincised by deep canyons with little hillslope erosion. This erosional reactivation is marked by a relatively high hypsometric integral (Fig. 5b, I=0.5).

4.3. Eroded volumes and uncertainties

For San Andrés Basin. The volume determined by the BTH method, for the smallest radius (L=3040, Table 1), is 30% greater than that determined by the IDW method. One can note as well that the error due to the BTH method is about five times higher than that of the IDW method. Figure 7 clearly shows the cause of these differences: while the profile of the interpolation using IDW is very close to the morphological marker (DEM profile) that of the BTH displays a very marked stair effect consistently located above the two other profiles. For the San Andrés Basin, the IDW reconstruction better fits this smoothed landscape surface (Fig. 5b, I=0.35) where hillslope erosion is important.

For El Salado Basin. The volume evaluated by interpolation of the pediments (≈29 km^3) is slightly smaller than that evaluated by the BTH function (≈32 km^3). However, the error due to the BTH application is half that using the IDW interpolation method (Table 1). This suggests that where the incised surface approximates a simple inclined plane with a localized canyon incision that narrows upstream, the BTH method is more accurate than the IDW method.

TABLE 1. COMPARISON OF IDW AND BTH DETERMINATIONS.

	San Andrés Basin				El Salado Basin			
Method	**EV (km^3)**	**AD (m/m^2)**	**Ac (%) (BTH)**	**RMSE (m)**	**EV (km^3)**	**AD (m/m^2)**	**Ac (%) (BTH)**	**RMSE (m)**
IDW	77.048	73.750	-	4.97	29.349	124.687	-	20.39
BTH San Andrés L = 3040 m El Salado L = 2960 m	100.911	96.592	5.017	22.44	32.690	138.879	2.061	9.17
L = 9920 m	256.491	245.514	-	200.83	-	-	-	-

Determinations of eroded volumes (**EV**), average denudations (**AD**=eroded volume/basin area), accuracy (**Ac**) and root mean square error (**RMSE**) for the San Andrés and the El Salado basins. The accurancy for the 'Top Hat' application is determined by about 80 m of imprecision in the selection of the structuring element.

4.4. Long-term denudation rates

To determine the long-term denudation rates we used the method best adapted to morphology *i.e*., the IDW eroded volume for the San Andrés watershed, and the BTH eroded volume for the El Salado Basin. Uncertainties in the eroded volume have been calculated by error propagation considering the error grid previously discussed. Final uncertainties in the long-term denudation rate during the last 10 Myr are determined by considering the average of the eroded volume uncertainties and by averaging the uncertainties associated with the published ages of the ignimbrite that seals the pedimentation surface.

The results are presented in Table 2: one can see that the denudation rate of the San Andrés Basin (≈7 m/Myr) is half that of the El Salado Basin (≈14 m/Myr), despite the basins being located adjacent to each other and having a similar relief and altitudes. Consequently, similar climate conditions can be supposed in both basins during the time span of basin denudation. Because no fault movements occur in these basins at this time they can not be invoked to explain the differences in the denudation rates (see above). Denudation rates and the factors controlling them depends on the drainage area of the basin; the denudation rate normally increasing with the size of the drainage area. Conversely, the San Andrés Basin (~1000 km^2) has a greater drainage area than the El Salado Basin (~250 km^2). The calculated long-term denudation rates from the eroded volume consider all the erosion components. The San Andrés Basin is characterized mainly by hillslope erosion, probably related to diffusive erosion processes of low intensity, which explains the weak denudation rate. The El Salado Basin has more intense erosion with stronger vertical incision. The understanding of the factors that control the difference in the erosive capacity between both basins is beyond the scope of this paper. However, this difference is most likely related to local factors such as differences in the lithology or the pre-Neogene tectonic configuration of the basins.

5. Discussion

In order to make comparisons with data collected by other methods certain remarks must be made. Our estimate of denudation rates considers all the erosion components that affect a pediment surface, and is based on the assumption that this pediment surface has remained stable during the last ~10 Myr. This assertion has recently been corroborated on the basis of combined measurements of cosmogenic ^{10}Be, ^{26}Al and ^{21}Ne, exposure ages Nishiizumi *et al*. (2005). These authors propose an age of 9 Ma and a maximum erosion rates <0.1 m/Myr on this surface. Thus, our estimates represent the overall denudation rate of the basins.

An important parameter in the long term erosion rate is the climate. We have compared the study region where the rainfall is about 40 mm/yr (Betancourt *et al*., 2000) to the Sierra Nevada (California) where 2 to 3 orders of magnitude more rainfall is recorded (200-1800 mm/y, Riebe *et al*., 2000). However, in the Sierra Nevada the erosion rates are only two to three times larger than those registered in the study region (Riebe *et al*., 2000). Thus, even if the climatic conditions are very different we maintain comparable erosion rates. This indicates that in the study region other factors besides the climate determine the erosion rates. Some 1000 km to the north of the study area, an important factor controlling the east-west variation of the Pliocene denudation rates along the Andean forearc is the orographically controlled pattern of rainfall (Kober *et al*., 2007). We propose that this orographic control also dominates the geomorphologic evolution and the long-term denudation rates in our study area. Indeed, the rainfall is about 130 mm/yr at the Salar de Pedernales east of the study area (Risacher *et al*., 1998)[3] (Fig.1); this greater rainfall being responsible for the runoff that allows the erosion to the west. Because erosion that gives rise to the current drainage basin systems begins at

TABLE 2. DENUDATION RATES AND ITS UNCERTAINTIES.

	San Andrés	El Salado
EV (km3)	77.04±15.1	32.15±2.6
DR (m/Myr)	7.33±1.6	13.59±1.9

Estimations and uncertainties of: eroded volume (**EV**) and long-term denudation rates (**DR**) for the San Andrés and El Salado basins.

[3] Risacher, F.; Alonso, H.; Salazar, C. 1998. Geoquímica de aguas en cuencas cerradas I, II, III regions, Chile. Convenio de Cooperación DGA-UCN-Orstom, 84 p.

~10 Ma (Riquelme *et al*., 2007), the influence of orographically controlled rainfall has dominated the landscape evolution at least for the last ~10 Ma. An orographically controlled rainfall pattern as a main factor affecting the Neogene geomorphologic evolution can be also proposed from the distribution and chronology of the supergene enrichment in the study area (Bissig and Riquelme, 2007).

Some 300 km to the north of our study area, in the central part of Atacama Desert, an average erosion rate of 7 m/Myr for the past 18 Myr was estimated (Scholl *et al*., 1970). The average erosion rate results from the estimation of the sediment volume in the Central Depression originating from the Andes range and deposited above an 18 Myr reference surface. Thus, this estimate also integrates all the erosion components. Near the Escondida mine (24º15´S), at the foot of the Precordillera, a maximum erosion rate of 9.5 m/Myr for the past 8.7 Myr was proposed by Alpers and Brimhall (1988). Despite the differences in the time span, these authors determine equivalent long-term denudation rates. Therefore, our proposed erosion rates for the San Andrés and the El Salado basins are largely in agreement with other reported estimates in the Atacama Desert. However, in the Precordillera and Western Cordillera of northern Atacama Desert -at latitude 18°S- long term denudation rates range up to 46 m/Myr during the Pliocene have been reported (Kober *et al*., 2007). Such great values in the denudation rates are related to a greater rainfall (up to 300 mm/yr) which, is due to the influx of the humid tropical air masses in the summer from the east (*e.g*., Amman *et al*., 2001). At present, a sharp decrease in the seasonality and intensity of rainfall from N to south is recorded for the Precordillera between ~22 to 24ºS (Betancourt *et al*., 2000). Therefore, our denudation rates suggest that the geomorphologic evolution of the study area was never affected by significant rainfall related to the humid tropical air masses, probably because they never extended as far south as latitude 26°S during the last ~10 Myr.

6. Conclusions

We have compared the use of BTH and IDW methods to estimate the long-term denudation rates for two drainage basins in the Central Andes: **(1)** the San Andrés and **(2)** the El Salado basins. In the San Andrés Basin, erosion leads to smoothed hillslopes with relatively low gradients. The selection of length L of the BTH function is thus very uncertain and can lead to non-realistic reconstructions. The IDW interpolation of these surfaces constitutes a more valuable approach when the selection of the values to be interpolated is appropriate. Considering the San Andrés case, the RMSE in the IDW reconstruction is only 22% of the minor error generated by the BTH reconstruction (L=3040 m, Table 1). The volumes calculated by the BTH function exceeds those calculated by IDW interpolation, although local underestimates are obtained for the smaller L. The IDW reconstruction considers the slope tendency of the preserved surface and generates surfaces that better approximate the pedimentation surface. The BTH function always generates flat surfaces which, in the case of a pedimentation surface, overestimates the real paleo-surface altitude. Therefore, we consider that the IDW interpolation generates a more realistic estimation of the eroded volume.

In contrast, in the El Salado Basin the volume estimated by using interpolation is similar to that of the Top Hat method. The application of the BTH is successful because the incised valleys narrow upstream which allows a good and rapid selection of the length L. In fact, the El Salado Basin displays an unusual landscape where two particular, and not necessarily frequent, characteristics are associated: a well defined incision and a good preservation of paleo-surfaces. These unusual characteristics are well recorded in the hypsometric curve of the basin, and the hypsometric curve and the hypsometric integral provide a useful quick-look estimate of which function is applicable (Fig. 4).

Since DEM errors propagate uncertainties when we rebuild paleo-surfaces, the construction of a grid error for the reconstructed surfaces allows the location of the uncertainties in our interpolated surface and its distribution in the landscape. The resulting volume has uncertainties derived from the DEM and the paleo-surface errors. The precision of our long term denudation rate is improved because it integrates these errors plus errors due to dating measurements.

The long term erosion rates obtained are in good agreement with those of other authors. The methods applied in this study allow a quick and precise estimation of long-term denudation rates and their

uncertainties. Furthermore, these methods provide reliable measurements in zones where direct measurement is impossible, or the measurement is expensive in terms of time and energy. They are applicable on landscapes characterized by large incised catchments where a reconstruction of paleosurfaces is possible, as that widely present in the chilean Central Andes.

Finally, after comparing our long-term denudation rates with those reported from other localities of the Atacama Desert and Sierra Nevada (California), we suggest that the denudation rates cannot be attributed to the current levels of rainfall, but may be explained by greater rainfall amounts as recorded to the east. This suggests that the geomorphologic evolution is dominated by an orographically controlled rainfall pattern which has affected the region at least for the last ~10 Myr. On the other hand, the low denudation rates and the preservation of remnants of the ~10 Ma pediment surface suggests that the study area was never affected by rainfall greater than recorded currently in the Precordillera at the latitude of Arica (18°S) which likely is associated to humid tropical air masses.

Acknowledgements

This research was supported by the Institute de Recherche pour le Développement, IRD, France and the ECOS-CONICYT collaboration Project (France-Chile): 'Modelamiento del comportamiento termo-mecánico y de la evolución geomorfológica del ante-arco del norte de Chile desde el Neógeno'. T. Bissig (Universidad Católica del Norte, Chile) is warmly thanked for the help with the English language and useful comments on an earlier draft of the manuscript. We are grateful to A. Hartley and J. Malavieille, as well as to an anonymous reviewer for constructive suggestions that greatly improved the manuscript.

References

Ahnert, F. 1970. Functional relationships between denudation, relief and uplift in large mid-latitude basins. American Journal of Science 268: 243-263.

Alpers, C.N.; Brimhall, G.H. 1988. Middle Miocene climatic change in the Atacama Desert, northern Chile: Evidence from supergene mineralization at La Escondida. Geological Society of America Bulletin 100: 1640-1656.

Amman, C.; Jenny, B.; Kammer, K.; Messerli, B. 2001. Late Quaternary Glacier response to humidity changes in the arid Andes of Chile. Palaeogeography, Palaeoclimatology, Palaeoecology 172: 313-326.

Beaumont, C.; Kamp, P.J.J.; Hamilton, J.; Fullsack, P. 1996. The continental collision zone, South Island, New Zealand: Comparison of geodynamical models and observations. Journal of Geophysical Research 101: 3333-3359.

Betancourt, J.L.; Latorre, C.; Rech, J.A.; Quade, J.; Rylander, K.A. 2000. A 22,000-year record of monsoonal precipitation from Northern Chile´s Atacama Desert. Science 289: 1542-1546.

Bissig, T.; Riquelme, R. 2007. Contrasting landscape evolution and development of supergene enrichment in the El Salvador, Potrerillos and la Coya porphyry Cu-Au districts, Northern Chile: Ores and Orogenesis: a Symposium Honoring the Career of William R. Dickinson, Program with Abstracts: 156-157. Tucson, Arizona.

Carretier, S.; Lucazeau, F. 2005. How does alluvial sedimentation at range fronts modify the erosional dynamics of mountain catchments? Basin Research 17: 361-381.

Coster, M.; Chermant, J.L. 1989. Précis d'analyse d'images, Centre National de la Recherche Scientifique, Paris: 521p.

Coultard, T.J. 2001. Landscape evolution models: a software review. Hydrological Processes 15: 165-173.

Fisher, N.I.; Lewis, T.; Embleton, B.J.J. 1987. Statistical analysis of spherical data. Cambridge University Press: 329 p.

Guyot, J.L. 1993. Hydrogéochimie des fleuves de l'Amazonie bolivienne. Collection études et thèses. Institut de Recherche pour le Développement (IRD), Paris: 261p.

Hartley, A.J.; Chong, G. 2002. Late Pliocene age for the Atacama Desert: Implications for the desertification of western South America. Geology 30 (1): 43-46.

Howard, A.D. 1997. Badland morphology and evolution: Interpretation using a simulation model. Earth Surface Processes and Landforms 22: 211-227.

Kober, F.; Ivy-Ochs, S.; Schulunegger, F.; Baur, H.; Kubik, P.W.; Wieler, R. 2007. Denudation rates and a topography-driven rainfall threshold in northern Chile: Multiple cosmogenic nuclide data and sediment budgets. Geomorphology 83: 97-120.

Maksaev, V.; Zentilli, M. 1999. Fission track thermochronology of Domeyko Cordillera, Northern Chile: implications for Andean tectonics and porphyry copper metallogenesis. Exploration and Mining Geology 8: 65-89.

Meigs, A.; Brozovic, N.; Johnson, M.L. 1999. Steady, balanced rates of uplift and erosion of the Santa Monica Mountains, California. Basin Research 11: 59-73.

Meyer, F. 1979. Cytologie quantitative et morphologie mathématique, Thèse de docteur ingénieur (Unpublished), Ecole des Mines, Paris.

Mortimer, 1973. The Cenozoic history of the southern Atacama Desert, Chile. Journal of the Geological Society of London 129: 505-526.

Nishiizumi, K.; Caffee, M.W.; Finkel, R.C.; Brimhall, G.; Mote, T. 2005. Remnants of a fossil alluvial fan

landscape of Miocene age in the Atacama Desert of northern Chile using cosmogenic nuclide exposure age dating. Earth and Planetary Science Letters 237 (3-4): 499-507.

Probst, J.L.; Suchet, A.P. 1992. Fluvial suspended sediment transport and mechanical erosion in the Maghreb (North Africa). Hydrological Science Journal 37: 621-637.

Randall, D.E.; Tomlinson, A.J.; Taylor, G.K. 2001. Paleomagnetically defined rotations from the Precordillera of northern Chile. Tectonics 20: 235-254.

Raymo, M.E.; Ruddiman, W.F.; Froelich, P.N. 1988. Influence of late Cenozoic mountain building on ocean geochemical cycles. Geology 16: 649-653.

Raymo, M.E.; Ruddiman, W.F. 1992. Tectonic forcing of late Cenozoic climate. Nature 359: 117-122.

Riebe, C.S.; Kirchner, J.W.; Granger, D.E.; Finkel, R.C. 2000. Minimal climatic control on erosion rates in the Sierra Nevada, California. Geology 29 (5): 447-450.

Riquelme, R.; Hérail, G.; Martinod, J.; Charrier, R.; Darrozes, J. 2007. Late Cenozoic geomorphologic signal of Andean forearc deformation and tilting associated with the uplift and climate changes of Southern Atacama Desert (26°S-28°S). Geomorphology 86: 283-306.

Rodríguez, F.; Maire, E.; Courjault-Radé, P.; Darrozes, J. 2002. The Black Top Hat function applied to a DEM: a tool to estimate recent incision in a mountainous watershed (Estibère Watershed, Central Pyrenees). Geophysical Research Letters. doi:10.1029/2001GL014412.

Serra, J. 1988. Image Analysis and Mathematical Morphology. Academic Press: 411 p. London.

Scholl, D.W.; Christensen, M.N.; Von Huene, R.; Marlow, M.S. 1970. Peru-Chile trench sediments and sea floor spreading. Geological Society of America Bulletin 81: 1339-1360.

Shepard D. 1968. A two-dimensional interpolation function for irregular-spaced data, Proceedings 23rd National conference of Association for Computing Mechinery (ACM): 517-524.

Sillitoe, R.H.; Mortimer, C.; Clark, A.H. 1968. A chronology of landform evolution and supergene mineral alteration, southern Atacama Desert, Chile. Institution of Mining and Metallurgy Transactions B 77: 166-169.

Sillitoe, R.; McKee, E. 1996. Age of supergene oxidation and enrichment in the Chilean Porphyry Copper Province. Economic Geology 91: 164-179.

Strahler, A. 1952. Hypsometric (area altitude) analysis of erosional topography. Geological Society of America Bulletin 63: 1117-1142.

Strahler, A. 1954. Quantitative geomorphology of erosional landscape. *In* International Geologic Congress No. 19. Algiers 13 (3): 341-354.

Tomlinson, A.J.; Mpodozis, C.; Cornejo, P.; Ramirez, C.F.; Dumitru, T. 1994. El Sistema de fallas Sierra Castillo-Agua Amarga: Transpresión sinistral eocena en la precordillera de Potrerillos-El Salvador. *In* Congreso Geológico Chileno, No. 7, Actas 2: 1459-1463.

Viers, G. 1967. Éléments de géomorphologie. Fernand Nathan: 207 p. París.

Whipple, K.X.; Tucker, G.E. 1999. Dynamics of the Stream Power River Incision Model: Implications for Height Limits of Mountain Ranges, Landscape Response Timescales and Research Needs. Journal Geophysical Research 104: 17661-17674.

Manuscript received: March 16, 2007; accepted: September 03, 2007.

APPENDIX A

Mathematical morphology concepts

***Set operation**:* The two basic operations in mathematical morphology are *dilatation* and *erosion* (Serra, 1988; Coster and Chermant, 1989). These operations involve the interaction between a set A representing the image under study and a set λ, called the *structuring element*, used to probe the image A. Let *A* and λ be subsets of a 2D plane.

The *translation* of *A* by *x* is defined as $A_x = \{c: c = a+x, \text{ for } a \in A\}$ (A1)

The *reflection* of λ is defined as $[\lambda] = \{x: x = -b, \text{ for } b \in \lambda\}$ (A2)

Dilation of the image *A* by the structuring element λ is given by
$\delta_\lambda(A) = \{x: [\lambda]_x \cap A \neq \emptyset\}$ (A3)

Erosion of the object *A* by a structuring element *B* is given by
$\varepsilon_\lambda(A) = \{x: \lambda_x \subseteq A\}$ (A4)

The image A and structuring element B need not be restricted to sets in the 2D plane, but could be defined in 1, 2, 3 or higher dimensions. On the other hand, *B* could be any shape. However, in order to simplify our explanation we consider the example where *A* is a rectangle and λ is a disc of radius R centred on the origin (Fig. A1). (Note that in this case λ is symmetric and [λ] = λ). Thus, the definitions become very intuitive: dilation expands an image object (Fig. A1a) and erosion shrinks it (Fig. A1b).

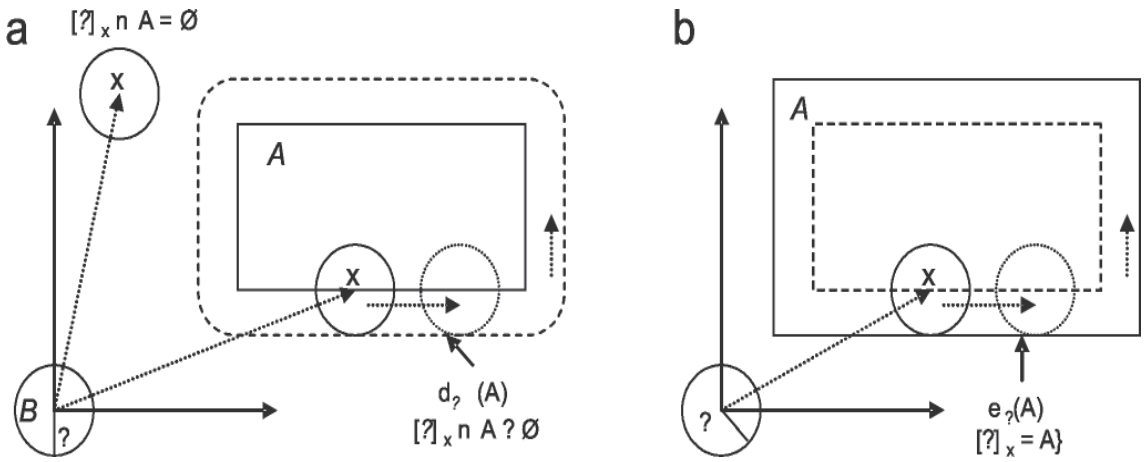

FIG. A1. **a.** The opening (dark dashed lines) of *A* (solid lines). The internal dashed structure is *A* eroded by λ.; **b.** The closing (dark dashed lines) of *A* (solid line) by the structuring element. The external dashed structure is *A* dilated by λ. In both cases λ is a disc.

Applications of morphological transformations: Dilation and erosion can be used in series to define two images transformations: *closing* and *opening*. The closing of *A* by λ is given by the dilation by λ, followed by the erosion by λ. Conversely, the opening is produced by the erosion of *A* by λ, followed by the dilation by λ**.** That is

$$C_{\lambda}(A) = \varepsilon_{\lambda}(\delta_{\lambda}(A)) \quad \text{- closing -} \qquad \text{(A5)}$$

$$O_{\lambda}(A) = \delta_{\lambda}(\varepsilon_{\lambda}(A)) \quad \text{- opening -} \qquad \text{(A6)}$$

Opening smooths a contour in an image, breaking narrow isthmuses and eliminating thin protrusions. It is obtained by taking the union of all translates of λ that fit inside *A*. Parts of *A* that are smaller than λ are removed (Fig. A2a). Closing tends to narrow smooth sections of contours, fusing narrow breaks and long thin gulfs, eliminating small holes, and filling gaps in contours (Fig. A2b).

Equivalence between Sets and Functions: A function can be viewed as a stack of decreasing sets. Each set is the intersection between the umbra of the function and a horizontal plane h.

$$X_h(f) = \{x: f(x) \geq h\} \Leftrightarrow f(x) = \sup\{h: x \in X_h(f)\} \qquad \text{(A7)}$$

Dilation and Erosion by a flat structuring Element: The dilation (erosion) of a function by a flat structuring element λ is introduced as the dilation (erosion) of each set $X_h(f)$ by λ. This definition leads to the following formulae:

$$\delta_{\lambda} f(X) = \sup\{f(x-y), y \in B\} \quad \text{- dilation-} \qquad \text{(A8)}$$

$$\varepsilon_{\lambda} f(X) = \inf\{f(x-y), y \in B\} \quad \text{-erosion-} \qquad \text{(A9)}$$

Erosion shrinks positive peaks. Peaks thinner that the structuring element disappear. It also expands the valleys and the sinks. Dilation produces dual effects.

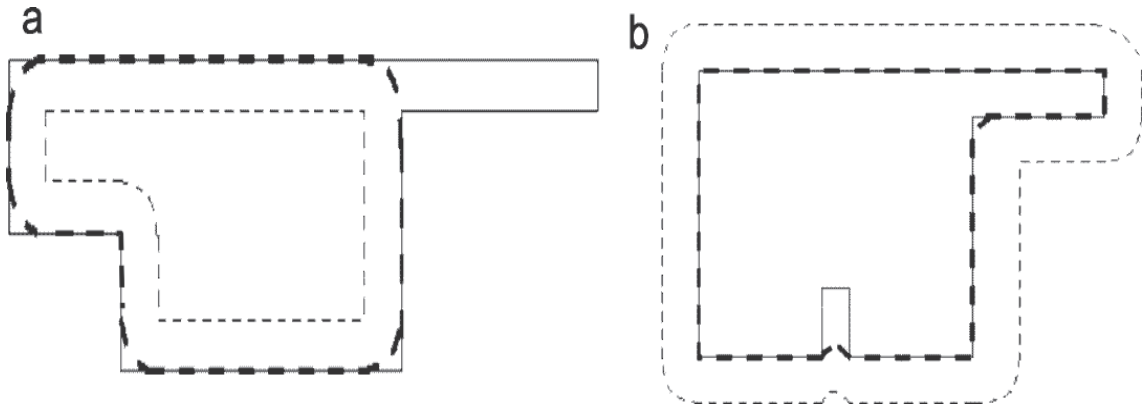

FIG. A2. **a.** *A* is dilated by the structuring element λ to give the external dashed shape; **b.** *A* is eroded by the structuring element λ to give the internal dashed shape.